Electrochimica Acta 91 (2013) 293–301

Contents lists available at SciVerse ScienceDirect

Electrochimica Acta

journal homepage: www.elsevier.com/locate/electacta

Thermodynamic properties of calcium–magnesium alloys determined by emf measurements

Jocelyn M. Newhouse, Sophie Poizeau, Hojong Kim, Brian L. Spatocco, Donald R. Sadoway*

Department of Materials Science and Engineering, Massachusetts Institute of Technology, 77 Massachusetts Avenue, Cambridge, MA 02139, USA

ARTICLE INFO

Article history:
Received 13 June 2012
Received in revised form
18 November 2012
Accepted 18 November 2012
Available online xxx

Keywords:
Calcium–magnesium alloys
Emf method
Thermodynamic properties
High temperature electrochemistry
Liquid metal battery

ABSTRACT

The thermodynamic properties of calcium–magnesium alloys were determined by electromotive force (emf) measurements using a Ca(in Bi)|CaF_2|Ca(in Mg) cell over the temperature range 713–1048 K. The activity and partial molar Gibbs free energy of calcium in magnesium were calculated for nine Ca–Mg alloys, calcium mole fractions varying from x_{Ca} = 0.01 to 0.80. Thermodynamic properties of magnesium in calcium and the molar Gibbs free energy of mixing were estimated using the Gibbs–Duhem relationship. In the all-liquid region at 1010 K, the activity of calcium in magnesium was found to range between 8.8×10^{-4} and 0.94 versus pure calcium. The molecular interaction volume model (MIVM) was used to model the activity coefficient of Ca and Mg in Ca–Mg liquid alloys. Based on this work, Ca–Mg alloys show promise as the negative electrode of a liquid metal battery in which calcium is the itinerant species: alloying with Mg results in both a decrease in operating temperature and suppression of Ca metal solubility in the molten salt electrolyte.

1. Introduction

Calcium is an attractive negative electrode material for use in electrochemical energy storage devices, such as liquid metal batteries [1,2], due to its low electronegativity, high earth abundance (comparable to that of iron) [3], and low cost (nearly one-third that of lithium) [4]. However, the use of molten calcium electrodes in liquid metal batteries presents two significant challenges: (1) the high melting temperature of elemental Ca (1115 K) requires high operating temperatures (>1115 K) resulting in increased difficulties associated with corrosion and thermal management [4] and (2) the high solubility of elemental Ca in molten salt electrolytes limits coulombic efficiency and gives rise to unacceptably high self-discharge currents. The present study explores Ca–Mg alloys as a means to decrease the melting temperature of the electrode material while minimally suppressing the potential from that of pure calcium.

Mitigating the solubility of calcium in molten salt electrolytes represents a more complex problem. The dissolution of Ca in molten salts decreases the coulombic efficiency by rendering the electrolyte electronically conductive [5] and providing a mechanism for self-discharge of a Ca-based liquid metal battery. The following three principal mechanisms have been proposed for the dissolution of Ca in molten salts [6]:

(1) formation of ions and creation of 'F-center' type solvated electrons

$$Ca \leftrightarrow Ca^{2+} + 2e^{-}, \quad (1)$$

(2) reaction with ionic species present in the salt and creation of monomeric subvalent ions

$$Ca + Ca^{2+} \leftrightarrow 2Ca^{+}, \quad (2)$$

(3) reaction with ionic species present in the salt and creation of dimeric subvalent ions

$$Ca + Ca^{2+} \leftrightarrow 2{Ca_2}^{2+}. \quad (3)$$

By Le Chatelier's principle, a decrease in the activity of Ca metal, a_{Ca}, through alloying would decrease its solubility in a molten salt in each case, assuming all other variables are constant (temperature, pressure, Ca^{2+} concentration, etc.). If mechanism (2) dominates, the solubility product is proportional to the square of the dissolved species (assuming a Henrian solution)

$$K_{sp} \propto \frac{[Ca^{+}]^2}{a_{Ca}[Ca^{2+}]} \quad (4)$$

and the concentration of dissolved Ca, $[Ca^{+}]$, is then proportional to the square root of Ca activity in the alloy,

$$[Ca^{+}] \propto \sqrt{a_{Ca}} \quad (5)$$

assuming $[Ca^{2+}]$ is constant. If either of mechanisms (1) and (3) is operative, then the concentration of dissolved Ca, $[Ca^{2+}]$ and

* Corresponding author. Tel.: +1 617 253 8468; fax: +1 617 253 5418.
E-mail address: dsadoway@mit.edu (D.R. Sadoway).

0013-4686/$ – see front matter © 2012 Elsevier Ltd. All rights reserved.
http://dx.doi.org/10.1016/j.electacta.2012.11.063

Ca_2^{2+} respectively, would be directly proportional to the activity of the metallic calcium. Much work has been done to elucidate the dominant mechanism for calcium dissolution [5–8]. Citing the increase in electronic conductivity of calcium-halides with addition of Ca metal, Dworkin et al. suggest mechanism (1) is the main source of metal solubility, with mechanism (3) playing a role at higher dissolved calcium concentrations [5]. Sharma measured the solubility of Ca in molten $CaCl_2$ for a variety of Ca–Cu alloys and concluded mechanism (1) or (3) was most probable based on the linear dependence of calcium solubility in the molten salt on a_{Ca} in the alloy [8]. Interestingly, in the case of Mg the solubility of the metal decreases in multi-cation molten salts from that observed with all Mg-halide salts [9]. Applying this observation to the Ca systems would suggest Ca^{2+} is a reactant, as opposed to a product, from which one would conclude mechanism (2) or (3) is most probable. Combining these results, mechanism (3) seems to be the dominant path for dissolution; however, the contribution of other mechanisms to Ca metal solubility cannot be ruled out [10].

Following from the preceding discussion, an alloy with very low Ca activity is the most promising candidate for suppressing Ca solubility in molten salt electrolytes; however, a lower Ca activity also reduces the cell voltage. Thus, the selection of a negative electrode alloy for battery applications must strike a balance between high cell voltage and low Ca solubility in the electrolyte. This study aims to assess the merits and limitations of Ca–Mg alloys as a negative electrode material for liquid metal batteries by measuring Ca activity in Mg using electromotive force (emf) measurements [1].

Previous determinations of the component activities in liquid Ca–Mg alloys were made by vapor pressure methods. Mashovets and Puchkov [11] measured the vapor pressure of Mg as a function of temperature from 1025 K to 1280 K over a wide range of alloy concentrations ($0.038 < x_{Ca} < 0.842$) using the saturation method, where an inert gas is passed over a sample at constant pressure, and the amount of sample transported by the gas is measured [12]. The vapor pressure of Ca was determined only for high calcium content alloys ($0.696 < x_{Ca} < 0.842$) because for dilute calcium alloys the partial pressure of calcium is negligible compared to that of magnesium. The temperature dependence of the partial pressures as well as the partial molar Gibbs free energy, entropy, and enthalpy of Ca and Mg were reported. Sommer [13] measured the vapor pressure of Mg for alloys with $x_{Ca} = 0.05–0.92$ at 1010 K using a modified Ruff technique, where the rate of mass loss is monitored as a function of pressure [12]. Sommer similarly reported only Ca vapor pressures for high calcium content alloys ($0.79 < x_{Ca} < 0.92$). By determining the calcium activity in Ca–Mg alloys at lower temperatures and over a wider range of alloy concentrations, the present study provides the fundamental understanding necessary for evaluating Ca–Mg alloys as negative electrode materials.

The thermodynamic assessment of Ca–Mg alloys is experimentally challenging due to the reactivity of calcium and the high vapor pressure of magnesium [14]. Electrochemical measurements are particularly problematic as calcium solubility in calcium-halide melts precludes their use as electrolytes. Furthermore, the widely used solid electrolyte CaF_2 [15] becomes a mixed conductor at high temperatures ($T > 873$ K) when in contact with high activity calcium ($a_{Ca} > 10^{-3}$ vs pure Ca) [6,16]. In this study, great care was taken to minimize issues arising from chemical compatibility and evaporation (see Section 2), while electronic conduction was minimized by using thick CaF_2 solid electrolytes and by ensuring short exposures of cells to high temperature.

The thermodynamic properties of Ca–Mg alloys were studied using the electrochemical cell

$$\mathrm{Ca(in\,Mg)|CaF_2|Ca(in\,Bi)}, \tag{6}$$

where various Ca–Mg alloys served as the working electrode (WE), a Ca–Bi alloy ($x_{Ca} = 0.35$) as the reference electrode (RE), and CaF_2 as a fluoride-conducting solid electrolyte [15]. Due to its superior chemical and emf stability [17] the Ca–Bi reference electrode consisting of a $Ca_{11}Bi_{10}(s)$ + liquid two-phase mixture was selected over pure calcium. The half-cell reactions for the cell are

$$\mathrm{RE: Ca(in\,Bi) + 2F^- \leftrightarrow CaF_2(s) + 2e^-} \tag{7}$$

$$\mathrm{WE: CaF_2(s) + 2e^- \leftrightarrow Ca(in\,Mg) + 2F^-} \tag{8}$$

and the overall cell reaction is

$$\mathrm{Ca(in\,Bi) \leftrightarrow Ca(in\,Mg)}. \tag{9}$$

The change in partial Gibbs free energy of calcium for the overall cell reaction is

$$\Delta_r \overline{G}_{Ca} = \overline{G}_{Ca(\text{in Mg})} - \overline{G}_{Ca(\text{in Bi})}, \tag{10}$$

where the partial molar Gibbs free energy of each component i, $\overline{G}_i$, versus the standard chemical potential of calcium, G°_{Ca} is given by

$$\overline{G}_i = G^{\circ}_{Ca} + RT\ln(a_i) \tag{11}$$

where R is the universal gas constant, T the absolute temperature, and a_i the activity. From the Nernst equation

$$\Delta\overline{G} = -zFE \tag{12}$$

and Eqs. (10) and (11) the measured electromotive force, E_{cell}, is related to the calcium activities in each electrode as follows:

$$E_{cell} = \frac{-\Delta_r \overline{G}_{ca}}{zF} = \frac{-RT}{zF}\ln\left(\frac{a_{Ca(\text{in Mg})}}{a_{Ca(\text{in Bi})}}\right), \tag{13}$$

where the number of electrons $z = 2$, and F is the Faraday constant.

2. Experimental

2.1. Materials

Alloy samples were prepared by arc melting (MAM-1, Edmund Buhler) calcium (99.99%, Aldrich) and magnesium (99.95%, Alfa Aesar) in an ultra-high purity argon atmosphere (99.999%, Airgas). The Ca–Bi (99.99%, Alfa Aesar) reference electrodes with $x_{Ca} = 0.35$ were prepared equivalently. After arc melting, samples were machined into cylinders and a hole drilled to accommodate the 1 mm Ø Mo (99.95%, Alfa Aesar) electrical lead. The chemical composition of each alloy was confirmed by an external vendor (Luvak, ASTM E1097-07) by direct current plasma atomic emission spectroscopy analysis (DCP-AES) according to ASTM E1097-07 standard (Table 1).

The solid electrolyte was prepared by thoroughly mixing 500 g of CaF_2 (Fischer Scientific, C89-500) with 150 mL of deionized water and 20 g of poly(vinyl alcohol) (Aldrich 341584-1KG). After drying in air, the powder (<850 μm) was pressed into a pellet 75 mm × 17 mm in diameter and thickness using 30 MPa of uniaxial pressure for 10 min. Seven wells were drilled in the green pellet as shown in Fig. 1a. Similarly, 19 mm Ø × 10 mm thick CaF_2 pellets (caps) were pressed and a 1.1 mm Ø hole made in the center. The electrolyte and caps were then fired in ambient environment for 12 h at 393 K, 12 h at 823 K, and 3 h at 1273 K to remove moisture, burn out binder, and sinter, respectively. The final pellets were white in color with approximately 98% theoretical density. For comparison, one cell test used a single crystal of CaF_2 (76 mm Ø × 19 mm, optical grade, CryLight Photonics, Inc.) with wells drilled for the alloys, as in Fig. 1a.

Table 1
Calcium mole fractions of the Ca–Mg alloys used as working electrodes for emf measurements, determined from weighed values and DCP-AES analysis. Samples analyzed by DCP-AES were taken from the arc-melted alloys before the experiments unless otherwise indicated.

Mole fraction, x_{Ca}	
Weighed	Analyzed
0.01	0.01
0.05	0.05, 0.05[a]
0.10	0.10
0.20	0.19
0.20	0.19
0.29	0.28
0.30	0.31, 0.30[a]
0.40	0.40
0.50	0.49[a]
0.50	0.45, 0.48
0.60	0.66[a], 0.56[a]
0.69	0.69[a]
0.80	0.80[a]

[a] Samples analyzed after emf measurement.

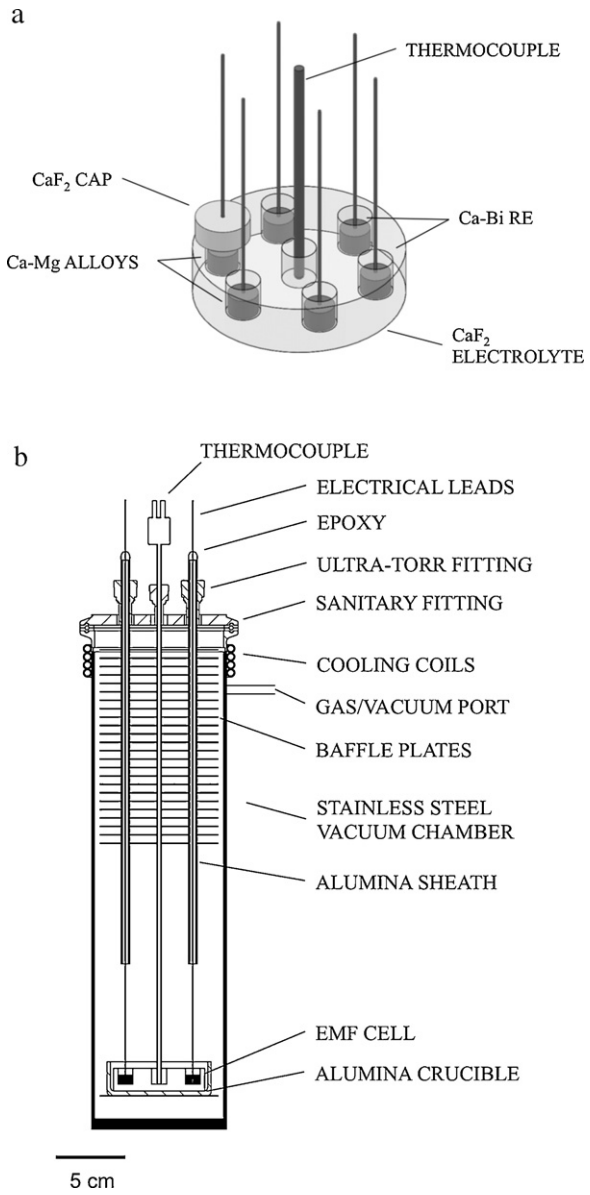

Fig. 1. Schematic of the experimental setup for emf measurements: (a) emf cell comprised of metal alloys contained in the CaF_2 solid electrolyte and (b) cross section of test vessel and chamber containing the emf cell.

Table 2
Emf data for the $Ca_{11}Bi_{10}$ + liquid two-phase region [17] used to determine $E_{RE} = (\partial E/\partial T)T + E(0\,K)$ at each measurement temperature.

T (K)	$\partial E/\partial T$ ($\times 10^5\,V^{-1}\,K^{-1}$)	$E(0\,K)$ (V)
700–767	-31 ± 1	1.05 ± 0.01
767–1050	-19.8 ± 0.3	0.958 ± 0.002

2.2. Test vessel

Emf measurements were carried out in a stainless steel vessel (Fig. 1b) sealed against external atmosphere. Seven ports were sealed with o-ring compression fittings, and stainless steel baffle plates provided thermal insulation. The emf cell was contained in an alumina crucible. Caps placed above each electrode minimized Mg vaporization. Alumina tubes sealed with epoxy electrically insulated the inert Mo electrode leads from the test vessel. The whole assembly was placed in a crucible furnace, and a vacuum pulled to test seals.

2.3. Procedure

The higher melting Ca–Bi REs ($T_m \sim 1100$ K) were pre-melted in the CaF_2 electrolyte at 1123 K to establish stable electrical contact between the REs, the electrolyte, and the leads without exposing the Ca–Mg alloys to high temperature. After the components had been dried at 393 K for at least 8 h under vacuum (~1 Pa) and then exposed to Ar, the temperature was increased to 1123 K and held there for 1 h under flowing Ar (ultra-high purity). Once cooled, the Ca–Mg electrodes were added to the assembly, and the test vessel was again evacuated at 393 K for more than 8 h, purged with Ar, and then brought to 873 K. All temperature changes were made with a ±5 K/min ramp rate.

Emf measurements were made at various temperatures by ramping between 713 K and 1048 K in 30 K steps, holding for at least 1 h at each temperature during the heating and cooling cycles. The temperature was recorded at the center of the electrolyte with a chromel–alumel (K-type) thermocouple (radial variation < 2 K). The emf between one RE and the other electrodes was measured sequentially for 120 s with a potentiostat–galvanostat (Autolab PGSTAT302N, Metrohm AG). When the temperature was constant (±<0.5 K), the stability of the emf signal was usually <0.1 mV, and there was good agreement between REs (<1 mV difference).

2.4. Reference electrodes

The two-phase Ca–Bi ($x_{Ca} = 0.35$) reference electrodes used in this study exhibited superior chemical and emf stability to pure calcium electrodes and are well characterized [17]. However, because pure calcium was not used as the reference electrode, the activity of Ca in the Ca–Mg alloys with respect to the standard state (pure calcium) cannot be determined from the cell potential alone (Eq. (13)). Using the data of Kim et al. (Table 2), the emf of the Ca–Bi reference electrode versus pure calcium

$$E_{RE} = \frac{-RT}{2F} \ln\left(\frac{a_{Ca\,(in\,Bi)}}{a_{Ca(s)}}\right) \tag{14}$$

can be calculated at each temperature from a linear fit of the data

$$E_{RE} = \left(\frac{\partial E}{\partial T}\right) T + E(0\,K) \tag{15}$$

with a precision of ±5 mV [17]. The emf of the working electrode with respect to pure calcium

$$E_{WE} = \frac{-RT}{2F} \ln\left(\frac{a_{Ca\,(in\,Mg)}}{a_{Ca(s)}}\right) \tag{16}$$

can then be calculated at each temperature from the measured cell potential (Eq. (13)) and the determined reference electrode emf

$$E_{WE} = E_{cell} + E_{RE}. \quad (17)$$

This result is used to calculate the activity of calcium in the Ca–Mg alloy WEs and the partial molar Gibbs free energy of Ca (Eq. (12)).

Throughout this work, the standard state of calcium is taken as the high-temperature solid phase, Ca(cr, $Im\bar{3}m$), and all values are reported with respect to this standard state. Notation going forward will be simplified as follows: $E_{WE} \rightarrow E$ and $X_{Ca(in\,Mg)} \rightarrow X_{Ca}$, where X is a generic thermodynamic variable.

2.5. Experimental error

The experimental sources of error in the determination of E arise from uncertainties in temperature, composition, and the calibration of the Ca–Bi ($x_{Ca} = 0.35$) reference electrode. With uncertainty in temperature less than 0.5% and that in concentration less than 1%, the ~5 mV uncertainty from the determination of E_{RE} dominates the error in the converted emf and, hence, the derived thermodynamic quantities. For low Ca concentrations the measured value of emf is great enough that this uncertainty introduces 2–5% error; however, at higher Ca concentrations the emf values range from $E = 0$ to 50 mV and the 5 mV uncertainty has a much more deleterious effect on the quality of the measurement.

3. Results and discussion

The emf values of Ca–Mg alloy concentrations between $x_{Ca} = 0.01$ and 0.8 were measured using an electrochemical cell of the configuration described by Eq. (6) with either sintered or single-crystal CaF_2. Compiled data from tests with a sintered CaF_2 electrolyte are presented in Fig. 2, referenced to Ca(s) according to Eq. (17). As seen in Fig. 2, the data collected during heating (every 30 K) follow the same trend as those collected during cooling (offset by 15 K), indicating thermal equilibrium at each step and minimal concentration change due to vaporization. Discontinuities in slope are apparent and indicate phase transformations. For $x_{Ca} < 0.33$, the values of emf for each alloy merge into distinct liquid + solid two-phase regions for alloy compositions on either side of the eutectic ($x_{Ca} \sim 0.10$). On the high Ca side of the intermetallic ($0.49 < x_{Ca} < 0.80$) the measured potentials (typically <20 mV) become obscured by measurement error (±5 mV) below 850 K, making the two-phase regions difficult to distinguish (Fig. 2b). The negative emf of the $x_{Ca} = 0.80$ alloy in the Ca(s) + liquid two-phase region ($T < 925$ K) is within error of the expected value, 0 mV versus Ca(s). Transition temperatures determined from slope changes in the emf trace are superimposed on the accepted phase diagram (Fig. 3) [18] and agree well.

The high-temperature data ($T > 900$ K) from the CaF_2 single crystal electrolyte test were reproducible and consistent with those obtained with the sintered electrolyte. At lower temperatures the single-crystal data were not consistent upon heating and cooling, possibly due to decreased electrolyte conductivity or poor electrode/electrolyte contact. These low-temperature data were excluded from analysis.

Above the liquidus temperature the emf data are observed to vary linearly with temperature, consistent with the combined Nernst and Gibbs–Helmholtz relation

$$E = -\frac{\Delta\bar{H}_{Ca}}{2F} + \frac{\Delta\bar{S}_{Ca}}{2F}T \quad (18)$$

where $\Delta\bar{H}_{Ca}$ and $\Delta\bar{S}_{Ca}$ are the partial molar enthalpy and entropy of Ca, respectively. Linear fits of emf versus temperature for those emf data in the single-phase region are reported in Table 3.

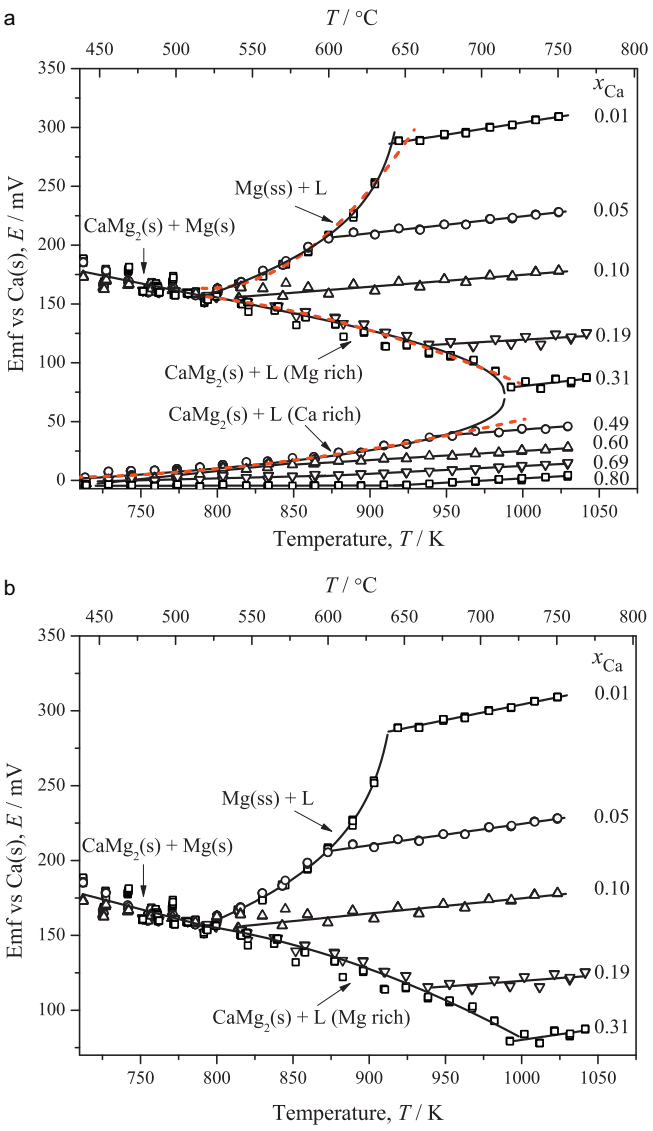

Fig. 2. Electromotive force as a function of temperature for electrochemical cells of the type Ca–Bi(s + l)|CaF_2|Ca(in Mg) referenced to Ca(s). Ca–Mg concentrations range from (a) $x_{Ca} = 0.01$–0.80, (b) $x_{Ca} = 0.49$–0.80. Solid lines are linear fits to the single-phase data and non-linear fits using Eqs. (22) and (23). Dashed lines are non-linear fits using Eq. (24) from the literature.

Table 3
Linear fits to emf E versus temperature T data for $x_{Ca} = 0.01$–0.80 in single-phase regions. Valid temperature ranges are indicated.

x_{Ca}	T (K)	$\partial E/\partial T$ ($\times 10^5$ V^{-1} K^{-1})[1]	E(0 K) ($\times 10^2$ V^{-1})
0.01	920–1020	20.7 ± 0.5	9.8 ± 0.5
0.05	875–1020	14.4 ± 0.4	8.4 ± 0.5
0.10	845–1020	10.1 ± 0.7	7.4 ± 0.7
0.19	940–1040	8 ± 2	4 ± 2
0.19[a]	940–1030	11.7 ± 0.8	−0.9 ± 0.7
0.29[a]	990–1030	13 ± 2	−4 ± 2
0.31	995–1040	15 ± 4	−7 ± 4
0.40[a]	970–1030	11 ± 1	−5 ± 1
0.48[a]	955–1030	9.1 ± 0.8	−4.4 ± 0.8
0.49	940–1030	10 ± 1	−5 ± 1
0.60	880–1030	7.8 ± 0.2	−5.1 ± 0.1
0.69	880–1030	6.6 ± 0.2	−4.1 ± 0.2
0.80	925–1030	7.2 ± 0.3	−7.0 ± 0.3

[a] Data from test with single crystal electrolyte.

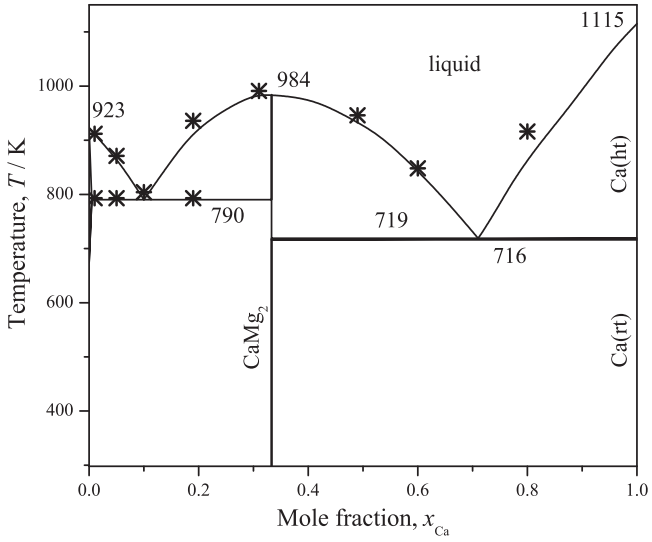

Fig. 3. Phase diagram of the Ca–Mg system [18] with the transition temperatures determined from emf measurements indicated (✱).

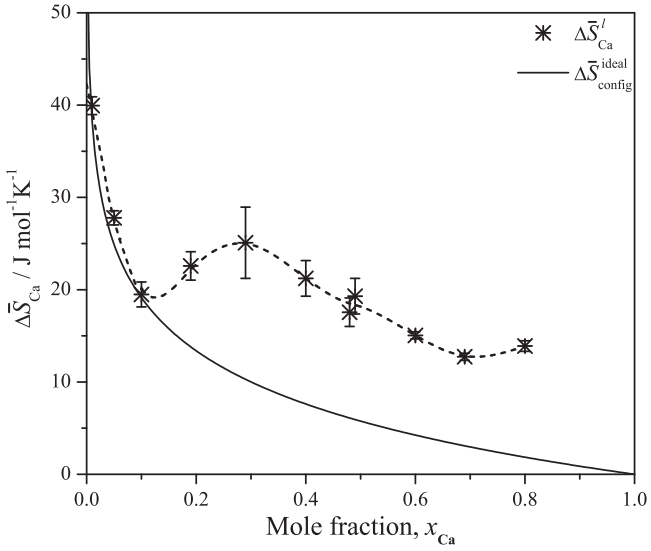

Fig. 4. The partial molar entropy of calcium in the liquid phase compared with the configurational entropy of an ideal binary solution. Error bars correspond to the error in the linear fits (Table 3).

Conversely, the emf trace with temperature exhibits curvature in the liquid + solid two-phase regions (Fig. 2), suggesting $\Delta\overline{H}_{Ca}$ and/or $\Delta\overline{S}_{Ca}$ varies with temperature. In a liquid + solid two-phase region, the composition of the liquid, at least, is a function of temperature, imparting the configurational entropy

$$\Delta\overline{S}_{Ca,config} = -R\ln(x_{ca}) \tag{19}$$

with apparent temperature dependence. In contrast, in a single-phase region the composition of the alloy does not change with temperature; therefore, $\Delta\overline{S}_{Ca,config}$ is invariant with temperature. On the assumption that the main contribution to $\Delta\overline{S}_{Ca}$ is configurational entropy (validity of assumption discussed below) the non-linear temperature dependence of the emf can be modeled as

$$E = -\frac{\Delta\overline{H}_{Ca}}{2F} - \frac{RT}{2F}\ln(x_{Ca}(T)). \tag{20}$$

Because the two phases are assumed to be in equilibrium, i.e., $\Delta\overline{G}_{Ca}$ is equivalent in each, the $\Delta\overline{S}_{Ca,config}$ of either phase can be modeled. In the Mg(ss) + L two-phase region the configurational entropy of the solid solution, $\Delta\overline{S}^{ss}_{Ca,config}$, was expressed in terms of a linear variation of x_{Ca} with temperature. This gives

$$x_{Ca} = \frac{x^{max}_{Ca,ss}}{T_m - T_e}(T_m - T) \tag{21}$$

where $x^{max}_{Ca,ss}$ is the solubility limit of Ca in the Mg solid solution, T_m the melting point of Mg (923 K), and T_e the eutectic temperature (790 K). Inserting this expression into Eq. (20) gives

$$E = A - BT\ln(T_m - T) + CT \tag{22}$$

where A can be interpreted as $-\Delta\overline{H}^{ss}_{Ca}/2F$, B as R/2F, and C as $(-R/2F)\ln(x^{max}_{Ca,ss}/(T_m - T_e))$. A curve using this fit is shown in Fig. 2a, and the parameters are reported in Table 4. The predicted solubility limit from this analysis, $x^{max}_{Ca,ss} = 0.012 \pm 0.005$, is within error of the literature values (0.005–0.011 [19,20]), suggesting that the assumptions are reasonable and that Eq. (22) could be used in other systems to approximate solubility limits. The Mg(ss) + $CaMg_2$(s) two-phase region could conceivably use a similar model; however, the data are too noisy to support a non-linear fit.

For the $CaMg_2$ + L two-phase regions, the liquidus line must be used to find $x_{Ca}(T)$, and the resulting expression is more complicated. Fitting the liquidus [18] to a parabola gives an expression for the emf of the form

$$E = A - BT\ln(0.333 + C'\sqrt{T_m - T}) \tag{23}$$

where A is now $-\Delta\overline{H}^{l}_{Ca}/2F$, B is the same as in Eq. (22), 0.333 is x_{Ca} of the intermetallic, C' is found from the curvature of the liquidus line, and T_m is the melting temperature of the $CaMg_2$ intermetallic. Comparison of the emf fits derived above to one found in the literature [21,22],

$$E = A - BT\ln T + CT, \tag{24}$$

shows good agreement over the data range (Fig. 2, Table 4). However, differences are exposed when extrapolation towards the melting point of the solid phase is considered: the fits of the $CaMg_2$ + L two-phase data using Eq. (23) predict a convergence of the emf at the intermetallic melting temperature (988 K), whereas the fits of the same data using Eq. (24) converge at a much higher temperature (1038 K).

For the $CaMg_2$ + L two-phase regions, B differs from R/2F, suggesting configurational entropy is not the only entropic contribution, whereas for the Mg(ss) + L region B is set as $R/2F$, and the curve matches well. This discrepancy is consistent with the value of the partial molar entropy of calcium in the liquid, $\Delta\overline{S}^{l}_{Ca}$, calculated from the single-phase linear fits (Table 3). As seen in Fig. 4, at low calcium content the $\Delta\overline{S}^{l}_{Ca}$ is very close to the ideal configurational entropy (Eq. (19)), but as Ca concentration increases, the data deviate from the $\Delta\overline{S}_{Ca,config}$ curve, especially close to the intermetallic composition $x_{Ca} = 0.33$. It should be noted that $\Delta\overline{S}_{Ca,config}$ was calculated assuming that two species exist in the melt, which may not be the case [23].

The interpolated emf values at 773 K, 873 K, and 1010 K from all tests are plotted in Fig. 5 and reported in Table 5. At the highest temperature (1010 K) the emf decreases smoothly as x_{Ca} increases, corresponding to a single liquid phase over the entire composition range. In contrast, at lower temperatures there are plateaus in emf over limited composition ranges indicative of two-phase equilibria. These data suggest that a Ca–Mg alloy used as the negative electrode in an electrochemical cell below 1010 K would operate at a voltage of less than 50 mV different from that of pure Ca

Table 4
Non-linear fits to emf E versus temperature T data in two-phase regions. Mg(ss)+ Mg rich liquid was fit to Eq. (22), $E = A - BT\ln(T_m - T) + CT$, and the $CaMg_2$(s)+liquid two-phase regions where fit to Eq. (23), $E = A - BT\ln\left(0.3333 + C'\sqrt{T_m - T}\right)$. In each case, only two parameters were varied. For comparison, a three-parameters fit used in the literature, $E = A - BT\ln T + CT$, is included (Eq. (24)) [21,22]. For the solid-solid two-phase region, $CaMg_2$(s)+Mg(ss), a linear fit $E = A + CT$ was used.

2-Phase region	Equations	T (K)	A	B	C or C'	T_m[a]
$CaMg_2$(s)+Mg(ss)		700–800	0.366	–	-2.6×10^{-4}	–
Mg(ss)+L (Mg rich)	(22)	800–900	0.0051	4.3×10^{-5}[a]	4.0×10^{-4}	923
$CaMg_2$(s)+L (Mg rich)	(23)	800–980	−0.048	1.1×10^{-4}	−0.0167 [a]	988
$CaMg_2$(s)+L (Ca rich)	(23)	750–925	−0.018	8.2×10^{-5}	0.023 [a]	988
Mg(s)+L (Mg rich)	(24)	800–900	−0.82	1.4×10^{-3}	0.011	–
$CaMg_2$(s)+L (Mg rich)	(24)	800–980	−0.06	-1.2×10^{-4}	0.0167	–
$CaMg_2$(s)+L (Ca rich)	(24)	750–925	0.51	7.5×10^{-4}	-5.7×10^{-3}	–

[a] Fixed values.

Table 5
Measured emf E, activity of calcium a_{Ca}, and Gibbs–Duhem estimated activity of magnesium a_{Mg} at 773 K, 873 K, and 1010 K. Values from the MIVM fit for the activity of calcium $a_{Ca,calc}$ and magnesium $a_{Mg,calc}$ are included at 1010 K.

	773 K			873 K			1010 K				
x_{Ca}	E (mV)	a_{Ca}	a_{Mg}	E (mV)	a_{Ca}	a_{Mg}	E (mV)	a_{Ca}	$a_{Ca,calc}$	a_{Mg}	$a_{Mg,calc}$
0.01	167	6.6×10^{-3}	0.99	208	3.9×10^{-3}	0.99	306	8.8×10^{-4}	8.5×10^{-4}	0.99	0.99
0.05	163	7.5×10^{-3}	0.99	206	4.2×10^{-3}	0.99	226	5.6×10^{-3}	6.0×10^{-3}	0.94	0.94
0.10	161	8.0×10^{-3}	0.99	162	1.4×10^{-2}	0.90	176	1.8×10^{-2}	1.7×10^{-2}	0.86	0.86
0.19[b]	161	8.0×10^{-3}	0.99	133	2.9×10^{-2}	0.80	120	6.3×10^{-2}	–	–	–
0.19[a]	–	–	–	–	–	–	127	5.4×10^{-2}	5.5×10^{-2}	0.71	0.71
0.29[a]	–	–	–	–	–	–	93	0.12	0.12	0.55	0.57
0.31[b]	157	9.0×10^{-3}	0.94	132	3.0×10^{-2}	0.79	82	0.15	–	–	–
0.40[a]	–	–	–	–	–	–	65	0.22	0.24	0.39	0.39
0.48[a]	–	–	–	–	–	–	49	0.33	0.34	0.29	0.30
0.49	7.5	0.80	4.6×10^{-2}	21	0.57	0.11	44	0.36	0.35	0.28	0.29
0.60	3	0.91	3.9×10^{-2}	15	0.67	9.0×10^{-2}	26	0.55	0.50	0.18	0.19
0.69	1	0.97	3.5×10^{-2}	4	0.90	5.3×10^{-2}	13	0.74	0.62	0.11	0.13
0.80	−4.3	1.1	3.2×10^{-2}	−4.3	1.1	3.9×10^{-2}	2	0.94	0.77	5.2×10^{-2}	6.8×10^{-2}

[a] Data from test with single crystal electrolyte.
[b] Data excluded from Gibbs–Duhem analysis at 1010 K due to inconsistencies attributed to magnesium evaporation.

when $x_{Ca} > 0.49$, whereas use of a low calcium content Ca–Mg alloy ($x_{Ca} < 0.33$) would decrease the voltage by as much as 300 mV.

Thermodynamic data for the Ca–Mg system at 773 K, 873 K, and 1010 K are summarized in Table 5 and Fig. 6. The activity of Ca in the Ca–Mg alloys at each temperature and concentration (Fig. 6a) was calculated from the emf data according to the Nernst equation

$$a_{Ca} = \exp\left\{\frac{-2FE}{RT}\right\} \tag{25}$$

where the emf, E, is referenced to Ca(s) (Eq. (17)). As evident from the small voltage difference between Ca–Mg alloys with $x_{Ca} > 0.49$ and Ca(s) (Fig. 2b), these alloys maintain a high calcium activity ($a_{Ca} > 0.6$ vs Ca(s) at 1010 K) and hence would not be expected to appreciably decrease the solubility of calcium in molten-halide electrolytes from that of pure calcium. Conversely, the alloys with low Ca content ($x_{Ca} < 0.2$) exhibit much lower calcium activities and could decrease the solubility of calcium in the electrolyte by as much as three orders of magnitude due to the observed pronounced negative deviation from Raoultian ideality.

The activity of Mg in the Ca–Mg alloys was derived from the Gibbs–Duhem relationship [24]

$$\ln\gamma_{Mg} = -\frac{x_{Ca}}{x_{Mg}}\ln\gamma_{Ca} - \int_1^{x_{Mg}} \frac{\ln\gamma_{Ca}}{x_{Mg}^2}\,dx_{Mg} \tag{26}$$

where the activity coefficient of component i, γ_i, is defined by

$$a_i = \gamma_i x_i. \tag{27}$$

An interpolated (smoothed spline) fit was used for the $\ln\gamma_{Ca}$ data. From the Gibbs–Duhem integration, the partial molar Gibbs free energies of Ca and Mg

$$\Delta\bar{G}_i = -RT\ln(a_i) \tag{28}$$

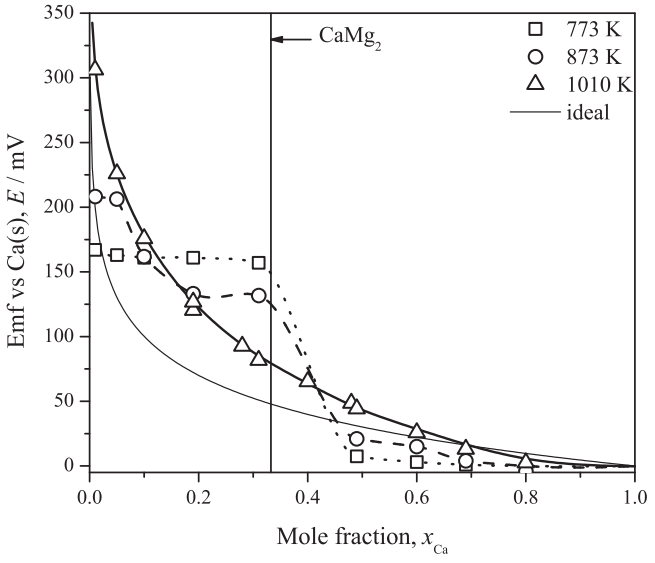

Fig. 5. Electromotive force as a function of concentration in Ca–Mg alloys at 773 K, 873 K, and 1010 K. The expected emf for an ideal solution at 1010 K is shown for comparison.

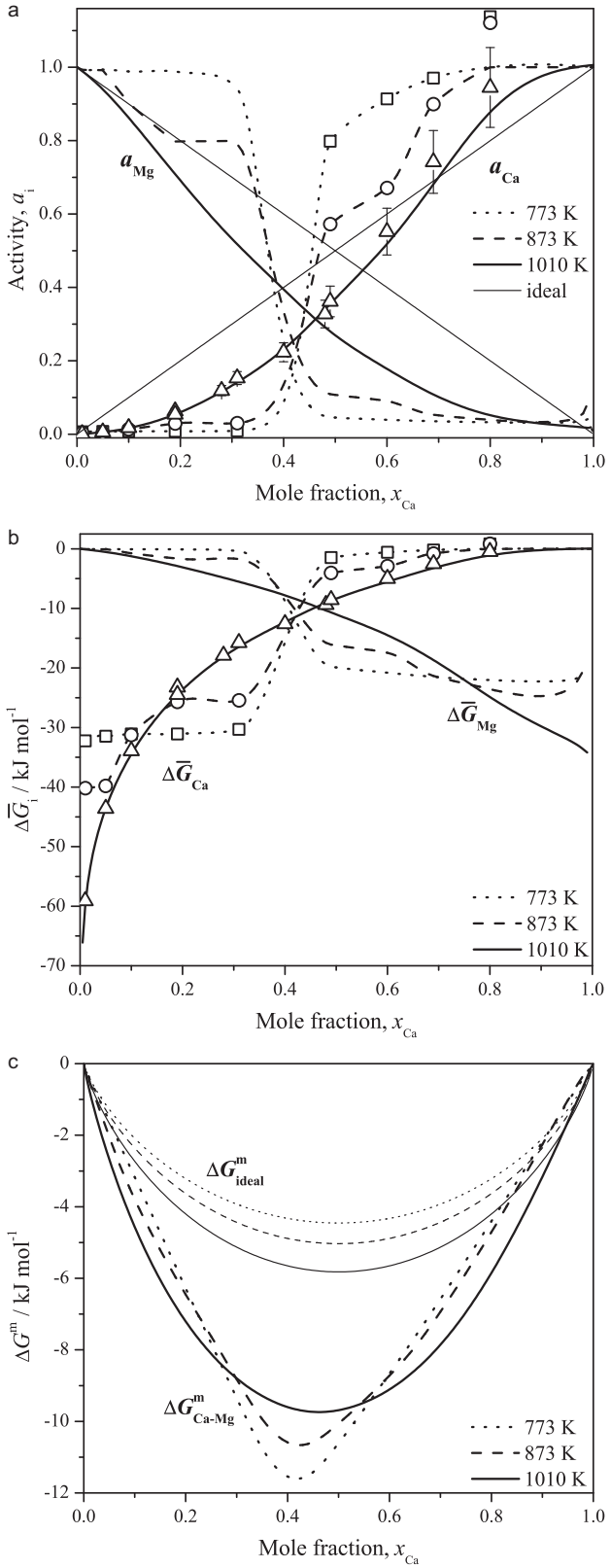

Fig. 6. Thermodynamic data derived from emf measurements for the Ca–Mg system at 773 K, 873 K, and 1010 K: (a) the activity of calcium a_{Ca} and magnesium a_{Mg}; (b) the change in partial molar Gibbs free energy of Ca $\Delta\bar{G}_{Ca}$ and Mg $\Delta\bar{G}_{Mg}$; (c) the integral molar Gibbs free energy of mixing ΔG^m_{Ca-Mg} compared to the ideal case ΔG^m_{ideal}. Error bars in (a) correspond to a ±5 mV error in the emf.

Table 6
Molar volume V_m and coordination number Z data [29] used for the MIVM model.

Species	V_m(m^3 mol^{-1})	Z
Ca	2.954×10^{-5}	10.33
Mg	1.560×10^{-5}	10.20

and the molar Gibbs free energy of mixing

$$\Delta G^m = x_{Ca}\Delta\bar{G}_{Ca} + x_{Mg}\Delta\bar{G}_{Mg} \quad (29)$$

were calculated and are presented in Fig. 6b and c. For this analysis, the negative emf of $x_{Ca} = 0.8$ (attributed to reference electrode calibration) was corrected to the expected value of 0 mV versus Ca(s) at 773 K and 873 K. At high temperature (1010 K), the sintered crystal data from $x_{Ca} = 0.19$ and 0.28 were excluded due to a noticeable decrease in the value of emf upon cooling, most likely caused by Mg evaporation.

Previously, Sommer modeled the thermodynamic properties of liquid Ca–Mg alloys using the regular association model [23,25], which fits the integral thermodynamic properties of mixing on the assumption of the presence of CaMg associates in the liquid. Although calcium and magnesium form an intermetallic compound, the strong similarity in their chemical behavior suggested that the molecular interaction volume model (MIVM) developed by Tao [26] may be appropriate for these alloys. Derived from statistical mechanics, the MIVM fits experimental data using only two parameters to represent the molar and partial molar thermodynamic properties of the liquid solution. The interaction parameters, B_{CaMg} and B_{MgCa}, were found by fitting the experimentally determined γ_{Ca} to Tao's equation for the activity coefficient of a species in a liquid i–j mixture

$$\ln\gamma_i = \ln\left(\frac{V_{mi}}{x_i V_{mi} + x_j V_{mj} B_{ji}}\right) + x_j\left(\frac{V_{mj}B_{ji}}{x_i V_{mi} + x_j V_{mj} B_{ji}} - \frac{V_{mi}B_{ij}}{x_j V_{mj} + x_i V_{mi} B_{ij}}\right) - \frac{x_j^2}{2}\left(\frac{Z_i B_{ji}^2 \ln B_{ji}}{(x_i + x_j B_{ji})^2} + \frac{Z_j B_{ij}^2 \ln B_{ij}}{(x_j + x_i B_{ij})^2}\right) \quad (30)$$

where the input parameters are the molar volume, V_m, and the atomic coordination number, Z, of the elemental liquids as defined

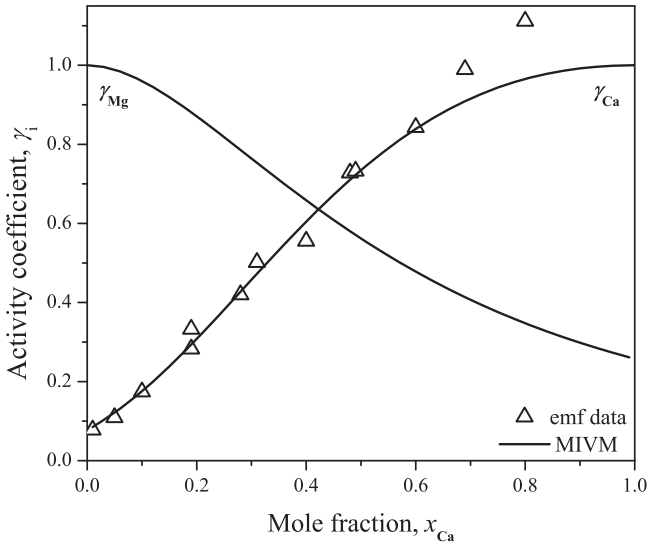

Fig. 7. The activity coefficient of calcium and magnesium at 1010 K calculated using the MIVM model and the fitted values.

by Tao (Table 6). The fit was optimized through minimization of the square of the error in predicted emf, $(E_{calc} - E_{exp})^2$, for all points (as in [27]). The optimized values for the interaction parameters are $B_{CaMg} = 1.532 \pm 0.001$ and $B_{MgCa} = 0.720 \pm 0.001$, which are indicative of almost random mixing in Ca–Mg liquid alloys. The modeled γ_{Ca} and a_{Ca} match well with the experimental values (Fig. 7, Table 5) suggesting that the MIVM is a suitable model for Ca–Mg alloys.

In Fig. 8, the thermodynamic properties determined from the emf results are compared to those obtained previously by vapor pressure measurements (Mashovets and Puchkov [11] and Sommer [13]). All values are reported at 1010 K, with those of Mashovets and Puchkov requiring extrapolation. The values from this study do not confirm the validity of one data set over the other but lie in between those from the previous measurements. Interestingly, at high Ca concentrations, the results of the present study as well as the data of Mashovets and Puchkov suggest a slight positive deviation from Raoultian ideality. The absence of this behavior in the data of Sommer could be explained by the reaction of Ca with container materials used for alloy preparation (alumina and graphite) [24,28]. Alternately, the positive deviation seen in this study can be attributed partially to experimental error. If the observed trend is representative of the thermodynamic properties of Ca–Mg alloys, it suggests that at high Ca content Ca–Ca interactions become more favorable than Ca–Mg interactions. This could explain why the MIVM does not reproduce the positive deviation at high calcium content: effectively the interaction parameters would have to be composition dependent, a feature absent from MIVM. If the goal of alloying were simply to lower the melting temperature of the negative electrode, this positive deviation would be a most welcome outcome. However, the higher than expected calcium activity hinders the ability of the Ca–Mg alloys to decrease solubility of Ca in the electrolyte.

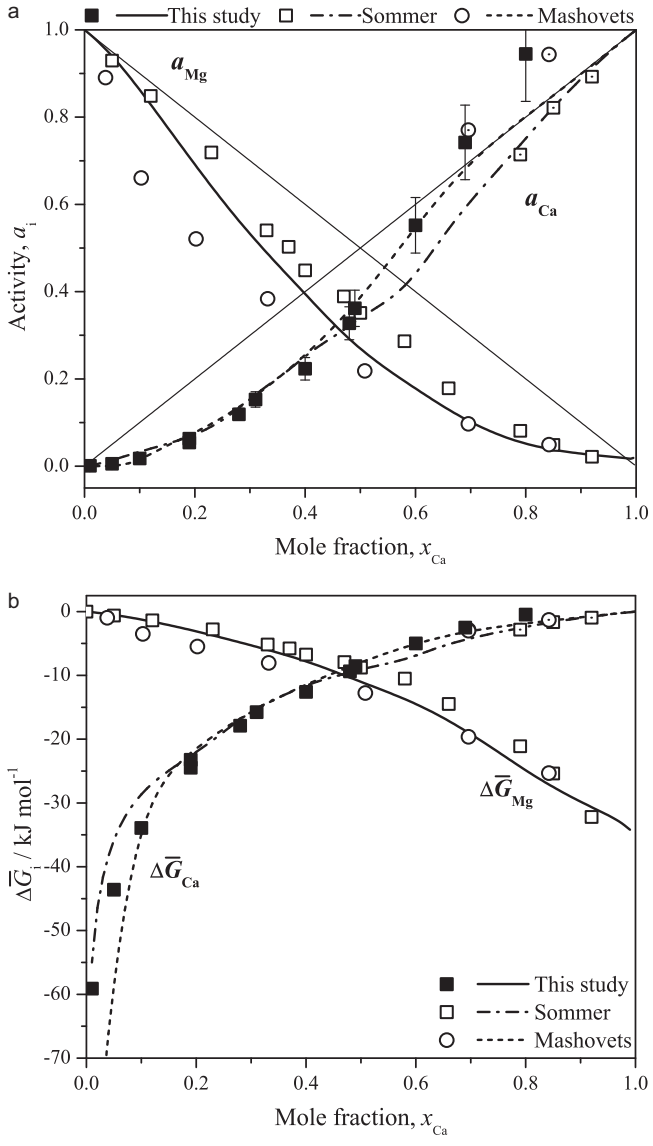

Fig. 8. Comparison of the literature values from Mashovets and Puchkov [11] and Sommer [13] to those found in this study of (a) the activity and (b) the partial molar Gibbs free energy of Ca and Mg. Experimental values (symbols) and values determined via Gibbs–Duhem integration (lines) are presented at 1010 K.

4. Conclusion

The results of this study have direct applicability to the use of Ca–Mg alloys as a negative electrode in all-liquid electrochemical energy storage devices. It was determined that a Ca–Mg alloy in the high-Ca eutectic region ($0.60 < x_{Ca} < 0.80$) would decrease the voltage by less than 30 mV, while allowing for operation below 950 K. However, the high activity of Ca in these alloys suggests that the solubility of metallic Ca in molten salt electrolytes would not be sufficiently suppressed. A negative electrode consisting of a Ca–Mg alloy on the low-Ca side of the intermetallic ($0.05 < x_{Ca} < 0.15$) would incur a voltage loss of $\sim$ 200 mV but could decrease the solubility of Ca in the molten salt by almost two orders of magnitude. Knowledge of the temperature dependence of Ca solubility in molten salt electrolytes would give further information as to which alloy would be the better candidate for a Ca–Mg negative electrode.

Acknowledgments

The financial support of the US Department of Energy, Advanced Research Projects Agency-Energy (Award No. DE-AR0000047) and TOTAL, S.A. is gratefully acknowledged. The authors would like to thank Dr. Dane Boysen and Rahul Malik for fruitful discussions and their helpful suggestions.

References

[1] D. Bradwell, D.R. Sadoway, Alkaline earth metal ion battery, US Patent 20,110,014,503, (2011).
[2] D. Bradwell, H. Kim, A.H.C. Sirk, D.R. Sadoway, Magnesium-antimony liquid metal battery for stationary energy storage, Journal of the American Chemical Society 134 (2012) 1895.
[3] G. Haxel, J. Hedrick, G. Orris, Rare earth elements – critical resources for high technology: US Geological Survey Fact Sheet 087-02, in, US Geological Survey (2002).
[4] H. Kim, D.A. Boysen, J.M. Newhouse, B.L. Spatocco, B. Chung, P.J. Burke, D.J. Bradwell, K. Jiang, A.A. Tomaszowska, K. Wang, W. Wei, L.A. Ortiz, S.A. Barriga, S.M. Poizeau, D.R. Sadoway, Liquid metal batteries: past, present and future. Chemical Reviews (2012) http://dx.doi.org/10.1021/cr/cr300205k
[5] A.S. Dworkin, M.A. Bredig, H.R. Bronstein, Ionic melts as solvents for electronic conductors, Discussions of the Faraday Society (1961) 188.
[6] M.A. Bredig, Mixtures of Metals with Molten Salts, Oak Ridge National Laboratory, Oak Ridge, TN, 1963.
[7] A.S. Dworkin, Hr. Bronstei, M.A. Bredig, Electrical conductivity of metals in their molten halides VII: alkaline earth metal systems, Journal of Physical Chemistry 70 (1966) 2384.
[8] R.A. Sharma, Solubilities of calcium in liquid calcium chloride in equilibrium with calcium-copper alloys, Journal of Physical Chemistry 74 (1970) 3896.
[9] E.A. Ukshe, N.G. Bukun, Dissolving of metals in molten halides, Uspekhi Khimii 30 (1961) 243.
[10] M.A. Bredig, in: O.R.N. Laboratory (Ed.), Mixtures of Metals with Molten Salts, Oak Ridge National Laboratory, Oak Ridge, Tennessee, 1963.
[11] V.P. Mashovets, L.V. Puchkov, Vapor pressure over liquid alloys in the system magnesium-calcium, Zhurnal Prikladnoi Khimii (Sankt-Peterburg, Russian Federation) 38 (1965) 1009.
[12] P.G. Wahlbeck, Comparison and interrelations for four methods of measurement of equilibrium vapor pressures at high temperatures, High Temperature Science 21 (1986) 189.

[13] F. Sommer, Determination of thermodynamic activities of liquid calcium-magnesium alloys using a modified Ruff method, Zeitschrift Fur Metallkunde 70 (1979) 545.
[14] R. Hultgren, P. D. Desai, D.T. Hawkins, M. Gleiser, K.K. Kelley, Selected values of the thermodynamic properties of binary alloys. National Standard Reference Data System, 1973.
[15] J.N. Pratt, Applications of solid electrolytes in thermodynamic studies of materials: a review, Metallurgical Transactions A 21A (1990) 1223.
[16] K. Kiukkola, C. Wagner, Galvanic cells for the determination of the standard molar free energy of formation of metal halides, oxides, and sulfides at elevated temperatures, Journal of the Electrochemical Society 104 (1957) 308.
[17] H. Kim, D.A. Boysen, D.J. Bradwell, B. Chung, K. Jiang, A.A. Tomaszowska, K. Wang, W. Wei, D.R. Sadoway, Thermodynamic properties of Ca-Bi alloys determined by emf measurements, Electrochimica Acta 60 (2012) 154.
[18] F. Islam, M. Medraj, The phase equilibria in the Mg-Ni-Ca system, Calphad – Computer Coupling of Phase Diagrams and Thermochemistry 29 (2005) 289.
[19] A. Nayeb-Hashemi, J. Clark, The Ca–Mg (calcium-magnesium) system, Journal of Phase Equilibria 8 (1987) 58.
[20] R. Agarwal, J.J. Lee, H.L. Lukas, F. Sommer, Sommer, Calorimetric measurements and thermodynamic optimization of the Ca–Mg system, Zeitschrift fur Metallkunde 86 (1995) 103.
[21] Y. Rao, B. Patil, Thermodynamic study of the Mg−Sb system, Metallurgical and Materials Transactions B 2 (1971) 1829.
[22] A. Petric, A. Pelton, M. Saboungi, Thermodynamic properties of liquid K-Bi alloys by electromotive force measurements, Journal of Physics F: Metal Physics 18 (1988) 1473.
[23] F. Sommer, Association model for the description of the thermodynamic functions of liquid alloys II: numerical treatment and results, Zeitschrift Fur Metallkunde 73 (1982) 77.
[24] D.R. Gaskell, Introduction to Metallurgical Thermodynamics, Scripta Publishing Co., Washington, DC, 1973.
[25] F. Sommer, Association model for the description of the thermodynamic functions of liquid alloys I: basic concepts, Zeitschrift Fur Metallkunde 73 (1982) 72.
[26] D.P. Tao, A new model of thermodynamics of liquid mixtures and its application to liquid alloys, Thermochimica Acta 363 (2000) 105.
[27] S. Poizeau, H. Kim, J.M. Newhouse, B.L. Spatocco, D.R. Sadoway, Determination and modeling of the thermodynamic properties of liquid calcium-antimony alloys, Electrochimica Acta 76 (2012) 8.
[28] E. Schurmann, H. Jacke, Melting equilibria in the system Fe–C–Ca, Steel Research 58 (1987) 399.
[29] D. Tao, Prediction of the coordination numbers of liquid metals, Metallurgical and Materials Transactions A 36 (2005) 3495.